

pubs.acs.org/NanoLett Letter

# Facile Size-Selective Defect Sealing in Large-Area Atomically Thin Graphene Membranes for Sub-Nanometer Scale Separations

Peifu Cheng, Mattigan M. Kelly, Nicole K. Moehring, Wonhee Ko, An-Ping Li, Juan Carlos Idrobo, Michael S. H. Boutilier, and Piran R. Kidambi\*



Cite This: Nano Lett. 2020, 20, 5951-5959



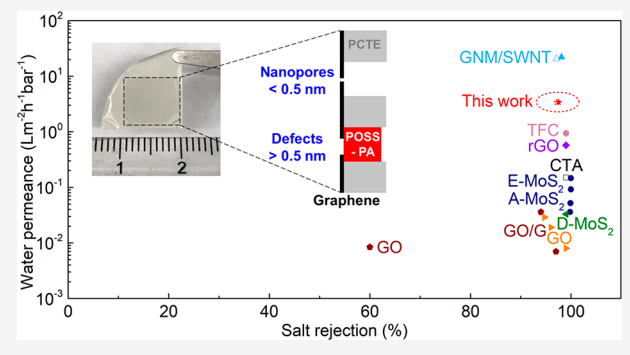
ACCESS

Metrics & More

Article Recommendations

s Supporting Information

**ABSTRACT:** Atomically thin graphene with a high-density of precise subnanometer pores represents the ideal membrane for ionic and molecular separations. However, a single large-nanopore can severely compromise membrane performance and differential etching between pre-existing defects/grain boundaries in graphene and pristine regions presents fundamental limitations. Here, we show for the first time that size-selective interfacial polymerization after high-density nanopore formation in graphene not only seals larger defects (>0.5 nm) and macroscopic tears but also successfully preserves the smaller subnanometer pores. Low-temperature growth followed by mild UV/ozone oxidation allows for facile and scalable formation of high-density  $(4-5.5 \times 10^{12} \text{ cm}^{-2})$  useful subnanometer pores in the



graphene lattice. We demonstrate scalable synthesis of fully functional centimeter-scale nanoporous atomically thin membranes (NATMs) with water ( $\sim$ 0.28 nm) permeance  $\sim$ 23× higher than commercially available membranes and excellent rejection to salt ions ( $\sim$ 0.66 nm, >97% rejection) as well as small organic molecules ( $\sim$ 0.7–1.5 nm,  $\sim$ 100% rejection) under forward osmosis.

**KEYWORDS:** nanoporous atomically thin membranes (NATMs), size-selective defect sealing, high density subnanometer pores, scalable graphene membranes, subnanometer separations, desalination

C ubnanometer scale separations are widely used across a range of chemical, biomedical, and industrial applications, for example, ionic and molecular separations via dialysis, nanofiltration, desalination, chemical and pharmaceutical purification, and beyond. Atomically thin 2D materials, such as graphene, represent the ideal membrane material to revolutionize subnanometer scale separations with atomic thinness, high mechanical strength, 1,2 and chemical robustness.<sup>3,4</sup> Although pristine graphene is impermeable even to helium atoms,<sup>5</sup> the introduction of precise high-density subnanometer pores in the graphene lattice could potentially enable the formation of nanoporous atomically thin membranes (NATMs) with very high solvent flux<sup>6</sup> (due to atomic thinness) while efficiently rejecting ions and solute molecules via molecular sieving. <sup>3,4,7</sup> However, even a single large defect in the graphene lattice over centimeter-scale areas can severely compromise NATM performance via nonselective leakage. 3,4,7 Forming precise subnanometer pores over large areas with a high density remains nontrivial and extremely challenging due to differential etching between pre-existing defects/grain boundaries and pristine regions.<sup>3,4</sup>,

Some studies have demonstrated graphene NATMs for ionic/molecular transport,  $^{8-11}$  gas separation,  $^{12-14}$  nanofiltration,  $^{7,15,16}$  and desalination. For example, Surwade et al.  $^{17,18}$  used oxygen plasma to introduce nanopores ( $\sim 10^{12}$  cm<sup>-2</sup>) in

~5 µm diameter monolayer graphene membranes and reported salt rejection during pervaporation of water (~1 ×  $10^6$  gm<sup>-2</sup> s<sup>-1</sup>, only one side of graphene was wetted) at 40 °C. Celebi et al.6 also reported water vapor transport through  $\sim$ 7.6–50 nm pores in graphene membranes but noted that capillarity prevented water transport when only one side of the membranes was wetted. O'Hern et al. 15 transferred centimeterscale graphene onto polycarbonate track etch (PCTE) supports and used a two-step procedure to seal nanoscale defects (via ALD of HfO<sub>2</sub>) as well as large tears (via interfacial polymerization). Subsequently, Ga ion bombardment to nucleate defects/nanopores followed by pore enlargement via oxidative etching allowed for nanofiltration of salts and small molecules. 15,16 However, nanopore creation via ion/electron bombardments in a microscope limits scalability. 15,16,19-Recently, Yang et al. used a carbon-nanotube mesh to support monolayer CVD graphene and further deposited a mesoporous silica layer on the other side of graphene and used it as a mask

Received: May 5, 2020 Revised: July 1, 2020 Published: July 6, 2020





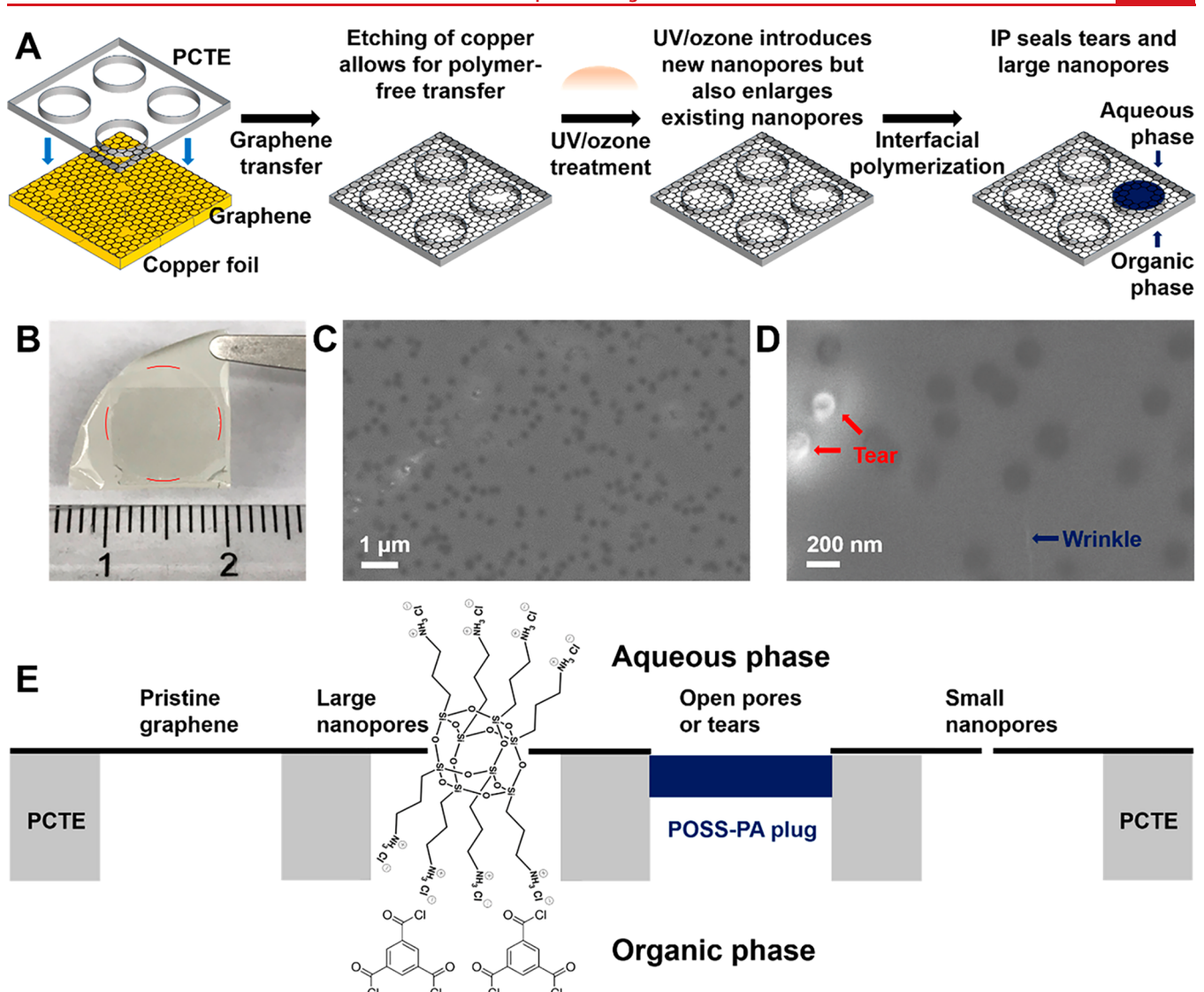


Figure 1. Fabrication and characterization of graphene nanoporous atomically thin membranes (NATMs). (A) Schematic of the fabrication process of graphene NATMs. Nanoporous graphene (NG) synthesized via CVD at 900 °C on Cu foil is pressed against PCTE support followed by etching of Cu. The PCTE provides adequate mechanical support and the well-defined, isolated cylindrical (~200 nm diameter) pore geometry allows for precise transport measurements without cross-talk from overlapping pores. <sup>8,9,15,27</sup> Subsequently, UV/ozone etching is used to introduce new defects but also enlarges existing intrinsic defects in the graphene lattice. Finally, facile and scalable interfacial polymerization with POSS (cage size ~0.5 nm) in the aqueous phase and TMC in hexane (organic phase) is used to seal tears and large nanopores in the graphene membrane via the formation of POSS–PA plugs/seals. (B) Optical image of graphene NATMs. The black square is the graphene area, and the red dashed circle represents the membrane region subjected to the interfacial polymerization process. (C,D) SEM images of graphene transferred on PCTE support. The dark circles indicate PCTE pores covered with suspended graphene. Red arrows show tears inevitably introduced during the mechanical pressing stage, and blue arrows show wrinkles in graphene. (E) Schematic of the mechanism for sealing tears and large nanopores (>0.5 nm) without blocking small nanopores (<0.5 nm) by interfacial polymerization. POSS and TMC are only expected to react and polymerize at large tears and/or large defects, forming POSS–PA plugs/seals. <sup>32,34</sup> Because the dimension of POSS is ~0.5–1.8 nm (~0.5 nm cage size), <sup>30</sup> the IP process does not block small nanopores <0.5 nm. Schematic of POSS and TMC redrawn based on refs 30 and 48.

to etch subnanometer pores via oxygen plasma. Their membranes showed high water transport (>20 L m $^{-2}$  h $^{-1}$  bar $^{-1}$ ), while blocking solute ions and the carbon-nanotube mesh provided adequate mechanical strength. However, the multistep processing and the use of a mesoporous SiO $_2$  mask and carbon nanotube mesh support only allow for limited scalability. Hence, the formation of high density, precise, subnanometer pores (0.28–0.66 nm) over large areas using facile and scalable processes remains an unresolved problem that fundamentally limits NATMs.  $^{3,4,7}$ 

Here, we report on scalable fabrication of fully functional graphene NATMs for ionic and molecular separations (Figure

1A) via novel size-selective interfacial polymerization (Figure 1E) after facile formation of high-density (4–5.5  $\times$   $10^{12}~cm^{-2})$  nanopores via low-temperature chemical vapor deposition (CVD) growth followed by mild UV/ozone oxidation.

## ■ RESULTS AND DISCUSSION

We specifically choose CVD graphene grown at  $\sim 900\,^{\circ}\mathrm{C}$  based on our extensive prior work \$^{11,25,26}\$ that evidenced the formation of subnanometer pores in the graphene lattice and transfer it onto polycarbonate track etch (PCTE) supports with  $\sim \! 200\,$  nm pores via a polymer-free transfer to ensure minimal surface contamination.  $^{8-11,15,26,27}$  Subsequently, mild

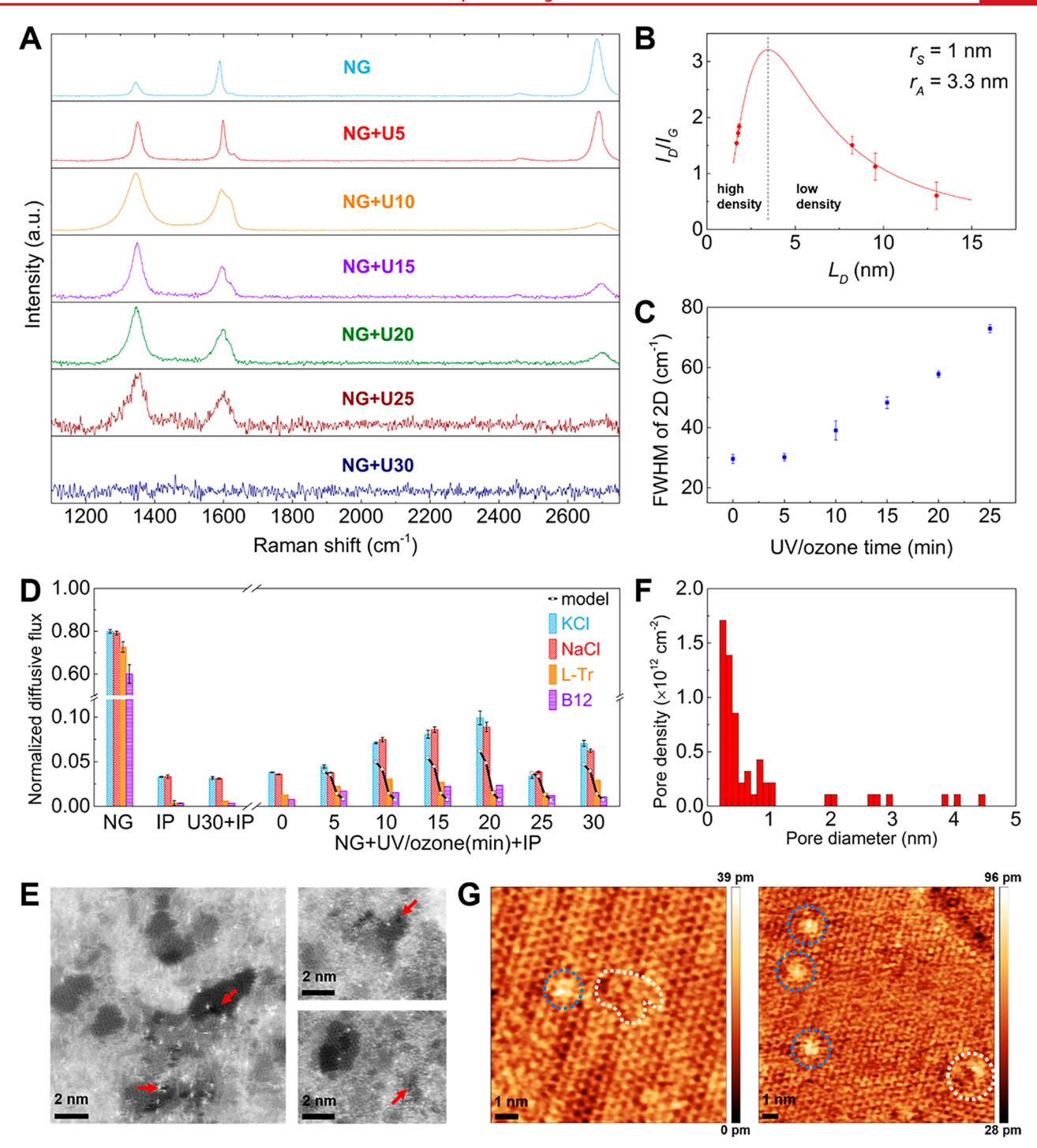


Figure 2. Assessment of subnanometer pores in the graphene lattice after UV/ozone etching and IP. (A) Raman spectra for 900 °C CVD graphene (NG) transferred to 300 nm SiO<sub>2</sub>/Si wafer exposed to UV/ozone etching for different times. Also see Supporting Information note 1. (B) The average interdefect distance ( $L_D$ , red markers) computed from the ratio of intensity of D and G peaks ( $I_D/I_G$ ). Curve is computed using  $I_D/I_G$ ,  $r_A$  = 3.3 nm (the radius of area surrounding the defect) and  $r_S$  = 1 nm (the radius of structural disorder) as described in Supporting Information note 1. <sup>37,38</sup> As-synthesized nanoporous graphene treated with UV/ozone for 0 to 10 min is in the low-defect-density regime, while longer UV/ozone exposure (more than 15 min) leads to a transition into the high-defect-density regime. (C) FWHM of 2D peak increases with increasing UV/ozone time. <sup>37,38</sup> (D) Diffusive flux normalized with respect to bare PCTE support membrane for different NATMs measured using four model solutes (KCl, ~0.66 nm; NaCl, ~0.66–0.716 nm; L-tryptophan, ~0.7–0.9 nm; Vitamin B12, ~1–1.5 nm). Black lines and open squares are the results of a solute diffusion model, which fit the experimental measurements well. (E) STEM images of as-synthesized nanoporous graphene after UV/ozone etching for 25 min indicates high-density subnanometer pores (red arrows indicate representative nanopores in different size ranges) and corresponding (F) measured pore size distribution. We note that there is no well-accepted/unique convention for defining the diameter of graphene nanopore <1 nm, hence we considered both the carbon electron radius (~0.065 nm) and carbon van der Waals (VDW) radius (~0.17 nm) and computed another pore size distribution (see Figure S2) which also indicated a majority of <0.5 nm nanopores. <sup>4,15,16</sup> (G) Atomic resolution STM images acquired on nanoporous graphene on Cu foil after UV/ozone etching for 25 min. Blue circles show the subnanometer defects while white curves represent nanometer scale pores.

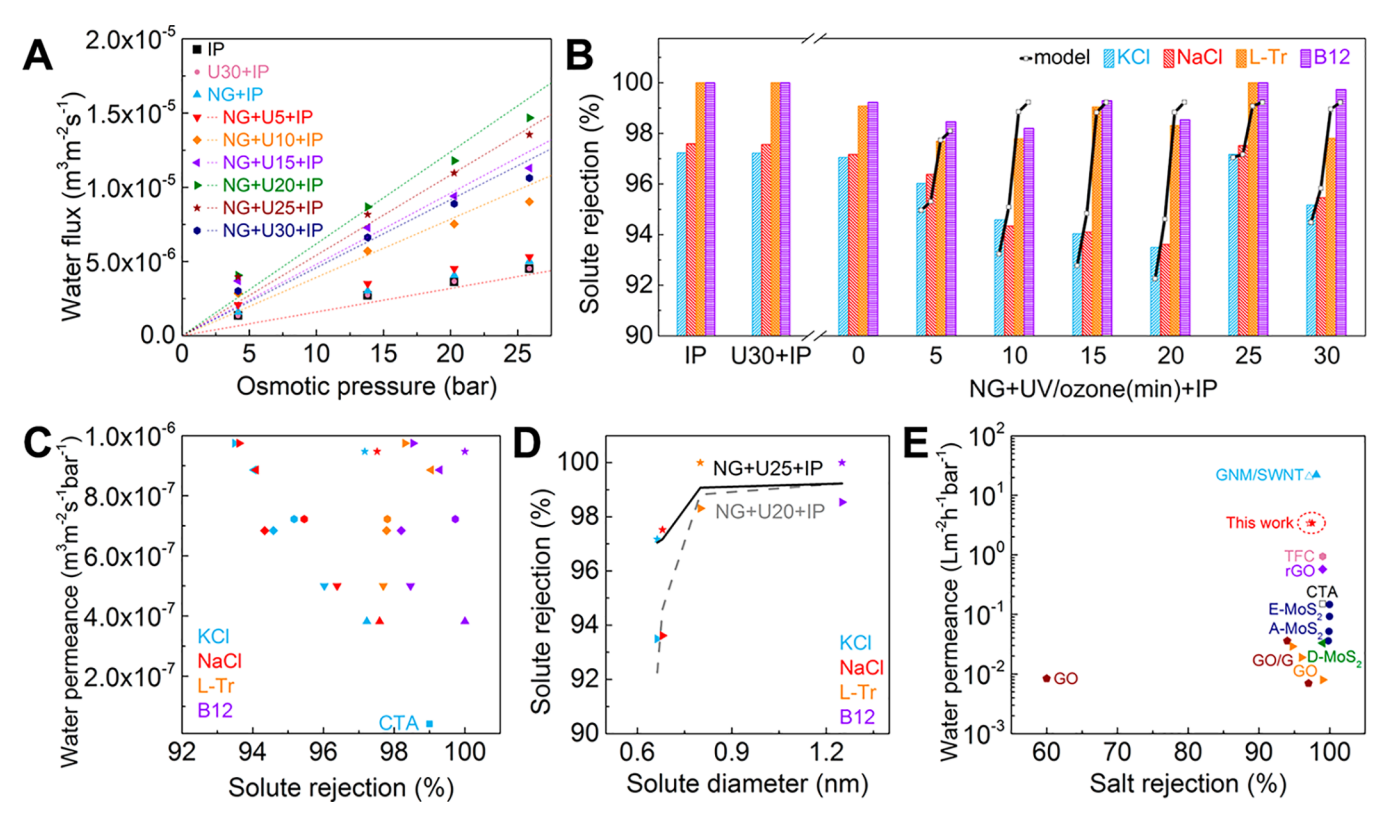


Figure 3. Evaluating the performance of graphene NATMs. (A) Water flux across graphene NATMs and PCTE supports (PCTE+IP) increases linearly with osmotic pressure. Dotted lines correspond to the water transport model. The water flux at the osmotic pressures of 4.2, 13.8, and 25.9 bar was measured during water transport experiments, while the water flux at the osmotic pressure of 20.3 bar was measured during solute transport experiments. Nanoporous graphene subjected to 20 min of UV/ozone etching (NG+U20+IP) exhibits the highest water flux, while NG+U25+IP membrane shows the second highest water flux. (B) Experimentally measured solute rejection through NATMs. NG+U20+IP membrane exhibits the lowest solute rejection result. In contrast, NG+U25+IP membrane shows the highest solute rejection result. Black lines and open squares show the transport model for solute rejection. (C) Water permeance and solute rejection through NATMs. Each symbol represents a membrane following the same symbol scheme in Figure 3A. Note water permeance takes into account the 9.4% porosity of PCTE supports (also see Figure S6). NG+U25+IP membrane has the second-highest water permeance (slightly lower than NG+U20+IP) but offers the highest solute rejection. L-Tr and B12 rejections of ~100% for NATMs with 0 and 25 min UV/ozone exposure results in some L-Tr (orange symbols) overlapping with B12 (violet symbols). (D) Solute rejections of NG+U20+IP (right triangle) and NG+U25+IP (star) membranes with respect to solute diameters (hydrated ion diameters of KCl and NaCl, molecular diameter of L-Tr and B12). Dashed and solid curves represent transport model for solute rejection. (E) Comparison of water-permeance and salt-rejection measured via forward osmosis for NATMs in this work (NG+U25+IP membrane) with other large-area membranes synthesized from 2D materials in literature, for example, graphene oxide (GO), 49 graphene oxide/ graphene (GO/G), 50 commercially available cellulose triacetate (CTA), 7 state-of-the-art advances in thin film composite (TFC) membranes, reduced graphene oxide (rGO),<sup>51</sup> Acetamide-functionalized MoS<sub>2</sub> (A-MoS<sub>2</sub>),<sup>52</sup> ethyl-2-ol-functionalized MoS<sub>2</sub> (E-MoS<sub>2</sub>),<sup>52</sup> dye-decorated MoS<sub>2</sub> (D-MoS<sub>2</sub>),<sup>53</sup> and graphene-nanomesh/single-walled carbon nanotube (GNM/SWNT)<sup>7</sup> membranes. We exclude the very high rates of water vapor transport ( $\sim$ 250 L m<sup>-2</sup> h<sup>-1</sup> bar<sup>-1</sup>) over  $\sim$ 5  $\mu$ m diameter graphene membranes, because they represent pervaporative water transport. Open symbols represent KCl rejection while filled symbols represent NaCl rejection.

etching conditions of UV/ozone exposure are used to enlarge existing defects in graphene as well as introduce additional nanopores in the graphene lattice. Finally, facile size-selective interfacial polymerization (IP) with octa-ammonium polyhedral-oligomeric-silsesquioxane (POSS,  $\sim$ 0.5 nm cage size) and trimesoyl chloride (TMC) is used to selectively seal tears and large nanopores (>0.5 nm) in graphene.  $^{10,15,31-33}$ 

Optical images of the synthesized NATMs (Figure 1B) show centimeter-scale nanoporous graphene (NG) on PCTE supports. Scanning electron microscopy (SEM) images further confirm successful transfer of graphene onto PCTE support (Figure 1C,D). The ~200 nm PCTE support pores covered with suspended graphene appear darker due to graphene's electrical conductivity, while uncovered PCTE pores (red arrows) underneath tears inevitably introduced during transfer

and handling appear bright due to polymer charging during SEM imaging.  $^{10,11,15,26,27}$ 

To seal such open PCTE support pores/tears in graphene and nanopores >0.5 nm in graphene after transfer to PCTE and UV/ozone etching, IP with POSS and TMC (Figure 1E) was performed. Because TMC is soluble in hexane but decomposes in water, and POSS is soluble in water but insoluble in hexane, the POSS molecules have to diffuse into hexane to react with TMC, that is, the interface for polymerization is pinned within the organic phase (within the PCTE support pores). Further, the transport of POSS (~0.5–1.8 nm) is sterically hindered through nanopores <0.5 nm in graphene, because the shortest dimension of POSS is ~0.5 nm (cage size, albeit the longest dimension of POSS is ~1.8 nm). Hence, we hypothesize that (i) small nanopores in graphene (<0.5 nm) would remain intact, (ii) nanopores in the range of 0.5–1.8 nm would be partially sealed, and (iii)

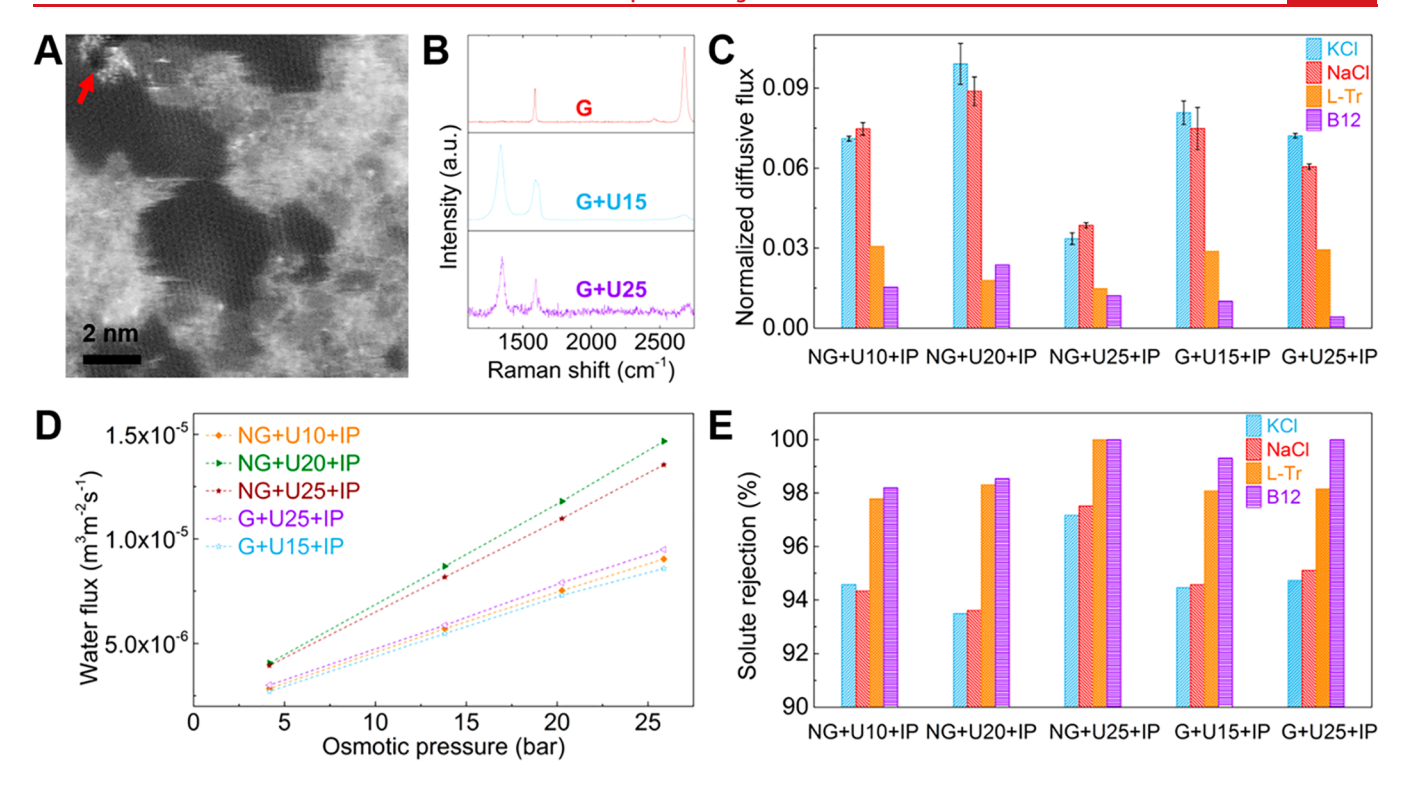


Figure 4. Characterization and evaluation of NATMs fabricated with high quality graphene (1050 °C CVD growth). (A) STEM image of high-quality graphene after UV/ozone treatment for 25 min indicates subnanometer pores, albeit with a density (see Figure S7) lower than nanoporous graphene (see Figure 2E,F). (B) Raman spectra of high quality graphene (note absence of D peak) transferred to 300 nm SiO<sub>2</sub>/Si wafer after different times of UV/ozone etching. (C) Diffusive flux normalized with respect to bare PCTE supports for NATMs with high quality graphene (G+U15+IP and G+U25+IP) and nanoporous graphene (NG+U15+IP and NG+U25+IP) with model solutes. (D) Water flux (E) solute rejection for high quality graphene NATMs compared with nanoporous graphene NATMs. These comparisons indicate that although NATMs fabricated using high quality graphene (G) could indeed be useful for ionic and molecular separations, the lower defect density results in lower performance compared to NATMs fabricated with nanoporous graphene (NG).

large nanopores (>1.8 nm), tears and open pores would be completely sealed via POSS–polyamide (PA). Considering the van der Waals diameter of water is  $\sim\!0.28$  nm, and hydrated diameters of K<sup>+</sup>, Cl<sup>-</sup>, and Na<sup>+</sup> are  $\sim\!0.662$ ,  $\sim\!0.664$ , and  $\sim\!0.716$  nm, respectively, our facile IP process with POSS (smallest dimension  $\sim\!0.5$  nm) could allow for graphene NATMs with high water permeability, while effectively rejecting larger ions and solutes.

Raman spectroscopy (Figure 2A and Supporting Information note 1) confirms the existence of defects in the assynthesized NG lattice  $^{11}$  as well as an increase in defects with increasing UV/ozone etch times, particularly for >15 min,  $^{10,25,26,31,35,36}$  as observed from the average interdefect distance ( $L_{\rm D}$ , see Figure 2B and Supporting Information note 1)  $^{37,38}$  and the full width at half-maximum (FWHM) of the 2D peak (Figure 2C).  $^{10,39}$ 

The performance of the NATMs for ionic and molecular separation was initially evaluated via diffusion-driven-flow (Figure 2D) and osmotic pressure-driven-flow measurements (Figure 3) using our customized experimental setup (Figure S1). Solutes and ions were specifically selected to confirm the formation of nanopores in the 0.28–0.66 nm size range in the NATMs, that is, KCl (salt, hydrated diameter of K<sup>+</sup> ~0.662 and Cl<sup>-</sup> ~0.664 nm), NaCl (hydrated diameters of Na<sup>+</sup> ~0.716 and Cl<sup>-</sup> ~0.664 nm), L-tryptophan (L-Tr, amino acid, ~0.7–0.9 nm, 204 Da), and Vitamin B12 (B12, vitamin, ~1–1.5 nm, 1355 Da).

Diffusive transport through the NATMs could arise from (i) selective transport through small nanopores in graphene, (ii)

nonselective leakage through tears and large nanopores in graphene, and (iii) leakage across the POSS-PA plugs. 27 The as-synthesized NG on PCTE supports without IP shows significant differences between normalized diffusive fluxes (normalized with respect to bare PCTE supports, Figure 2D) of KCl ( $\sim$ 80%) and B12 ( $\sim$ 60%), indicating the presence of subnanometer defects in the graphene lattice 11,26 in addition to nonselective diffusive transport across large tears and open PCTE pores. After IP, the as-synthesized NG membrane (NG +UV/ozone 0 min+IP in Figure 2D or NG+IP) shows significantly reduced normalized diffusive fluxes for all species (~3.5% for KCl and NaCl, <1% for L-Tr and B12), indicating IP with POSS-PA blocks most nanopores >0.66 nm along with any large tears and open PCTE pores in the NATMs. Control experiments with bare PCTE supports after IP (IP in Figure 2D) and PCTE supports after UV/ozone etching for 30 min (U30+IP in Figure 2D) after IP showed normalized diffusive fluxes of ~3% for KCl and NaCl and negligible leakage for L-Tr and B12. We attribute these leakages to transport through the POSS-PA plugs and note the negligible impact of UV/ozone etching on PCTE supports. Upon increasing UV/ozone etching times up to 20 min the normalized diffusive fluxes of KCl for NATMs systematically increases from  $\sim 3\%$  to  $\sim 10\%$  but decrease to  $\sim 3\%$  for 25 min and ~7% for 30 min. The normalized diffusive fluxes of NaCl show a similar trend. For L-Tr ( $\sim$ 0.7-0.9 nm) and B12 ( $\sim$ 1-1.5 nm) the normalized diffusive fluxes remain <3% for all the NATMs, further indicating the POSS-PA IP process effectively blocks nanopores >0.66 nm, along with any tears

or open PCTE support pores. Diffusion-driven-flow experiments with NATMs from different batches with similar processing (Figure S3) show fully consistent results indicating the reliability and reproducibility of the entire process including graphene synthesis, transfer, UV/ozone etching, and IP.

The measured ion diffusion rates were fitted to an analytical diffusion model (see detailed description in Supporting Information note 2) in which transport is approximated as occurring through an array of independent, parallel pores in a thin membrane separating reservoirs at different concentrations. The pores are approximated as following a log-normal distribution with the mean, standard deviation, and pore density selected to match the model to the measurements. Leakage is accounted for by adding the transport rates measured on nonetched membranes in the model. The model is able to reasonably fit the diffusion measurements (Figure 2D), providing further evidence that subnanometer pores created through graphene synthesis and UV/ozone etching are governing the measured diffusion rates.

Atomic resolution scanning transmission electron microscopy (STEM, Figure 2E) confirms the existence of nanopores in the as-synthesized nanoporous graphene lattice after 25 min of UV/ozone etching. The nanopore size distribution indicates that the vast majority of nanopores are <0.5 nm, with some nanopores in the 0.5–1 nm range and few large nanopores >1 nm (Figures 2F and S2).  $^{4,15,16,40}$  The overall nanopore density is  $\sim\!6.3\times10^{12}$  cm $^{-2}$ , while the effective pore densities after excluding nanopores >0.5 nm and >1.8 nm are  $\sim\!4\times10^{12}$  cm $^{-2}$  and  $\sim\!5.5\times10^{12}$  cm $^{-2}$ , respectively. These measured nanopore densities are in excellent agreement with the nanopore density of  $\sim\!8.1\times10^{12}$  cm $^{-2}$  obtained for 25 min UV/ozone etch time from the transport model fit (Table S1).

Interestingly, the nanopore densities for UV/ozone treated high quality graphene (Figures 4A and S7) were found to be lower than  $\sim 2.7 \times 10^{12}$  cm $^{-2}$ , indicating the efficacy of our approach at nucleating a high-density of nanopores via low-temperature CVD. Although we used a polymer-free procedure for transferring graphene to TEM grids for STEM imaging, unavoidable adventitious contaminants are typically seen to adhere on defects/nanopores in comparison to pristine regions (Figures 2E and 4A). We specifically avoided annealing in H<sub>2</sub> to reduce contaminants, since aggressive cleaning/etching/heating could alter the nanopore size distributions.

To further confirm the existence of subnanometer pores in graphene without transfer and minimal contamination, we also acquired scanning tunneling microscopy (STM) images of nanoporous graphene on Cu foil after UV/ozone etching for 25 min (Figure 2G). Bright defects marked by blue circles are subnanometer scale vacancy defects <sup>41,42</sup> and larger defects (~0.4–1.5 nm) marked by white dashed curves indicate nanometer-sized pores, <sup>41,42</sup> confirming the presence of nanopores in the graphene lattice.

Osmotic pressure-driven flow experiments for the synthesized graphene NATMs show an increase in water flux with increasing UV/ozone time from 0 to 20 min (Figure 3A, Table S4) and a linear increase in water flux with osmotic pressure (0–25 bar). A marginal reduction in water flux is observed for the 25 min UV/ozone exposure, followed by a further decrease at 30 min. Control measurements with bare PCTE supports (IP in Figures 3A and S5) and PCTE supports after 30 min UV/ozone exposure (U30+IP in Figure 3A) show significantly lower water flux indicating (a) the majority of the water

transport is through nanopores in graphene and (b) the near identical water flux values measured for the controls indicate minimal effect of UV/ozone etching on PCTE supports. Here we note that water transport across the NATMs could arise from (i) nanopores <0.66 nm in graphene, which could allow water to permeate while blocking salt ions, and (ii) large nanopores (0.66–1.8 nm), which give rise to the transport of water, salt ions, and small organic molecules.

Hence, in addition to water transport, we also measured rejection of model solutes (KCl, NaCl, L-Tr, and B12) after 24 h of osmotic pressure-driven water permeation through the synthesized NATMs (Figure 3B).7 The rejection of KCl and NaCl for the NATMs gradually decreases with increasing UV/ ozone exposure up to 20 min and then increases at 25 min (the highest salt rejection) before decreasing again at 30 min. The rejection of L-Tr and B12 in all NATMs remains >97.5% and >98.5%, respectively. These minimal leakages of L-Tr <2.5% and B12 <1.5% in the NATMs are attributed to a few unsealed large nanopores (0.66-1.8 nm). Control measurements with PCTE supports (IP in Figure 3B) and PCTE supports after 30 min UV/ozone exposure (U30+IP in Figure 3B) show solute rejection of KCl ~97%, NaCl ~97.5%, L-Tr ~100%, and B12 ~100%, indicating the efficacy of POSS-PA plugs/seals and represents the upper bound for salt rejection attainable (remaining is leakage through POSS-PA).

The permeance versus solute rejection (Figure 3C) allows for an unambiguous evaluation of the performance of the synthesized NATMs and is a well-known trade-off in conventional nanofiltration, ionic and molecular separation, and desalination membranes. 4,7 The NATM with 20 min UV/ ozone exposure (right facing triangles) showed the highest water permeance ( $\sim$ 9.8  $\times$  10<sup>-7</sup> m<sup>3</sup> m<sup>-2</sup> s<sup>-1</sup> bar<sup>-1</sup>) and the lowest solute rejection (KCl ~93%, NaCl ~93%, L-Tr ~98%, and B12 ~98%). However, NATM with 25 min UV/ozone exposure (star symbols) showed very high water permeance  $(\sim 9.5 \times 10^{-7} \text{ m}^3 \text{ m}^{-2} \text{ s}^{-1} \text{ bar}^{-1}$ , only marginally lower than NG + UV/ozone 20 min) and the highest solute rejection (~97% rejection of KCl and NaCl, 100% rejection of L-Tr and B12). These observations indicate the presence of nanopores >0.66 nm that were not fully sealed by POSS-PA in the NATM with 20 min UV/ozone etching. However, 25 min of UV/ozone enlarges the nanopores adequately to be effectively sealed by IP and results in marginally lower water flux (due to the loss of some nanopores via POSS-PA sealing) but results in much higher solute rejection. Overall, the solute rejections for NATMs with 20 and 25 min of UV/ozone increases with solute diameters (Figure 3D). However, the NATM with 20 min UV/ozone exposure has the largest fraction of relatively large nanopores (0.66-1.8 nm), while NATM with 25 min UV/ozone exposure has the largest fraction of subnanometer pores (<0.66 nm).

The transport model was extended to predict rates of water transport by forward osmosis and osmotically driven salt ion convection-diffusion across the membrane. Water flow rates through graphene pores were calculated from the correlation developed by Suk and Aluru<sup>43</sup> based on molecular dynamics simulation results. Salt convection-diffusion was modeled using approximate analytical expressions for convective and diffusive transport across a pore in a thin membrane and through a cylindrical PCTE membrane pore (see Supporting Information note 2). The transport model effectively captures the water flux (Figure 3A) and the dependence of ion rejection on diameter (Figure 3B,D) for the different UV/ozone etch times. We

emphasize that the same model pore size distribution and density have been used in all model curves at a given etch time (Figures 2D and 3A,B,D). Just as the measured rates of diffusion, osmosis, and salt convection-diffusion all arise from the same pore size distribution and density in the membrane, the model is able to use a single pore size distribution and density to explain the measured flow rates from these three different transport modes. This further supports the conclusion that the subnanometer pores in the graphene lattice are responsible for the measured salt diffusion, water flow rate, and salt rejection trends. The model's success in quantitatively explaining the experimental measurements makes it a very useful design tool for predicting membrane performance gains as the pore size distribution and density are tuned.

Taken together, the results from Raman spectroscopy (Figure 2A), diffusion-driven solute transport (Figure 2D), osmotic pressure-driven transport (Figure 3A), solute rejection (Figure 3B), and water permeance versus solute rejection (Figure 3C) indicate that the defect/nanopore density and size distribution range in graphene NATMs increases with UV/ ozone exposure via the formation of new defects as well as the enlargement of existing defects, respectively. As more defects form in the graphene lattice with increasing etch times (increasing water flux), the merging of individual defects leads to the formation of larger nanopores. With longer UV/ozone etching times, the larger nanopores (~0.5-1.8 nm) will eventually grow larger than >1.8 nm and will end up being sealed via IP. Our results indicate the highest salt rejection (>97%) and very high water flux ( $\sim$ 9.5  $\times$  10<sup>-7</sup> m<sup>3</sup> m<sup>-2</sup> s<sup>-1</sup> bar<sup>-1</sup>) for UV/ozone etch time corresponding to 25 min on the as-synthesized nanoporous graphene after IP (POSS cage ~0.5 nm and diagonal length ~1.8 nm), indicating the largest fraction of <0.66 nm nanopores.

A detailed comparison of the water permeance and salt rejection (KCl and NaCl) of the NATMs with 25 min UV/ ozone etching with other ionic and molecular separation membranes reported in the literature is presented in Figure 3E. Our NATMs exhibit a higher water permeance than all membranes in the literature, except for graphene supported on single-walled carbon nanotubes (SWNTs). We attribute this to the higher transport resistance for the ~200 nm diameter PCTE support pores compared to the porous SWNT mesh. Hence, the water permeance of NATMs could potentially be further improved by replacing PCTE supports with a lower resistance hierarchically porous support in future studies.<sup>11</sup> Interestingly, when compared with the commercially available cellulose triacetate membrane (CTA)<sup>7</sup> and state-of-the-art advances in thin film composite (TFC) membranes, 44 the water permeance of our NATMs under forward osmosis (~3.5 L m<sup>-2</sup> h<sup>-1</sup> bar<sup>-1</sup>) is already up to 23 times and 3.7 times higher, respectively, with comparable salt rejection. 45-47

Finally, we also fabricated NATMs with high quality graphene synthesized at 1050 °C (D peak ~1350 cm $^{-1}$  is not seen in the Raman spectrum, Figure 4B). However, the nanopore density of ~2.7  $\times$   $10^{12}$  cm $^{-2}$  (Figures 4A and S7) obtained via UV/ozone etching of high quality graphene for 25 min is significantly lower than with the as-synthesized ~900 °C nanoporous graphene of ~6.3  $\times$   $10^{12}$  cm $^{-2}$  (Figure 2F) resulting in lower performance (Figure 4C–E). These observations indicate the effectiveness of the combination of NG via low temperature CVD growth (~900 °C) and UV/ozone etching in creating a high density of subnanometer pores in the graphene lattice for NATMs.

#### CONCLUSION

In summary, we have developed a novel, facile, and scalable approach to synthesize fully functional large-area graphene NATMs for ionic and molecular separations. The combination of low-temperature CVD growth of NG, subsequent UV/ ozone etching, and size-selective IP allows for facile synthesis of NATMs with high-density subnanometer pores. To the best of our knowledge, this is the first demonstration of sizeselective defect sealing for NATMs and the obtained water permeance is ~23× higher than commercially available water treatment/desalination membranes, along with salt rejection >97% and small molecule rejection ~100%. Further improvements in water permeance are expected with lower resistance hierarchically porous supports.<sup>11</sup> Our work provides a facile and scalable route to overcome fundamental limitations in the development of NATMs for ionic/molecular separations. These advances coupled with our prior work on roll-to-roll graphene synthesis<sup>31</sup> and facile polymer support casting<sup>11,31</sup> could enable NATMs to progress toward practical applications and enable transformative advances in subnanometer scale ionic and molecular separations relevant to chemical processing, biochemical/biological research, medical/therapeutic research, pharmaceuticals purification, and other industrial applications.

### ASSOCIATED CONTENT

# Supporting Information

The Supporting Information is available free of charge at https://pubs.acs.org/doi/10.1021/acs.nanolett.0c01934.

Experimental section; Figure S1, experimental setup; Figures S2 and S7, calculated pore size distributions adjusted to the carbon electron radius and carbon van der Waals radius; Figure S3, solute diffusion comparison between membranes; Figure S4, water flux through graphene membrane when draw solution is placed on the graphene side versus the PCTE membrane side; Figure S5, water level change on the feed side for PCTE +IP membrane during water flux measurement; Figure S6, performance of NATMs; Table S1, model fit pore density values; Table S2 and Table S3, comparison of performance among different FO membranes reported in the literature and this work; Table S4, solutions in the feed and permeate side for solute diffusion, water transport, and solute rejection experiments; Note 1, assessment of Raman spectra of graphene lattice after UV/ozone etch; Note 2, Table S5 and Figures S8-S10, transport model (PDF)

# AUTHOR INFORMATION

# **Corresponding Author**

Piran R. Kidambi — Department of Chemical and Biomolecular Engineering and Interdisciplinary Materials Science Program, Vanderbilt University, Nashville, Tennessee 37212, United States; © orcid.org/0000-0003-1546-5014; Email: piran.kidambi@vanderbilt.edu

#### **Authors**

**Peifu Cheng** — Department of Chemical and Biomolecular Engineering, Vanderbilt University, Nashville, Tennessee 37212, United States

- Mattigan M. Kelly Department of Chemical and Biomolecular Engineering, Vanderbilt University, Nashville, Tennessee 37212, United States
- Nicole K. Moehring Department of Chemical and Biomolecular Engineering and Interdisciplinary Materials Science Program, Vanderbilt University, Nashville, Tennessee 37212, United States
- Wonhee Ko Center for Nanophase Materials Sciences, Oak Ridge National Laboratory, Oak Ridge, Tennessee 37831, United States
- An-Ping Li Center for Nanophase Materials Sciences, Oak Ridge National Laboratory, Oak Ridge, Tennessee 37831, United States; orcid.org/0000-0003-4400-7493
- Juan Carlos Idrobo Center for Nanophase Materials Sciences, Oak Ridge National Laboratory, Oak Ridge, Tennessee 37831, United States
- Michael S. H. Boutilier Department of Chemical and Biochemical Engineering, Western University, London, Ontario N6A 5B9, Canada

Complete contact information is available at: https://pubs.acs.org/10.1021/acs.nanolett.0c01934

#### **Author Contributions**

P.R.K. conceived and supervised the project. P.C. fabricated graphene membranes, performed Raman characterization, carried out the diffusion and osmotic pressure-driven measurements, and analyzed the results. M.M.K. contributed to water and solute transport measurements. N.K.M. prepared high quality CVD graphene. W.K. and A.-P.L. performed scanning tunneling microscopy measurements. J.C.I. performed scanning transmission electron microscopy measurements. M.S.H.B. performed the transport modeling and wrote the corresponding part in manuscript. All the authors were involved in analysis and discussions of the results. P.C. and P.R.K. wrote and edited the manuscript with input form all authors.

# Notes

The authors declare no competing financial interest.

#### ACKNOWLEDGMENTS

The use of Vanderbilt Institute of Nanoscale Science and Engineering CORE facilities and Prof. Carlos Silvera Batista's Lab for UV/ozone etching is acknowledged. This work was supported by ACS PRF Grant Number 59267-DNI10, NSF CAREER award #1944134, and faculty start-up funds to P.R.K. from Vanderbilt University. The STEM and STM imaging were performed at the Center for Nanophase Materials Sciences at Oak Ridge National Laboratory, a U.S. Department of Energy Office of Science User Facility.

#### REFERENCES

- (1) Cohen-Tanugi, D.; Grossman, J. C. Mechanical Strength of Nanoporous Graphene as a Desalination Membrane. *Nano Lett.* **2014**, *14* (11), 6171–6178.
- (2) Wang, L.; Williams, C. M.; Boutilier, M. S. H.; Kidambi, P. R.; Karnik, R. Single-Layer Graphene Membranes Withstand Ultrahigh Applied Pressure. *Nano Lett.* **2017**, *17* (5), 3081–3088.
- (3) Prozorovska, L.; Kidambi, P. R. State-of-the-Art and Future Prospects for Atomically Thin Membranes from 2D Materials. *Adv. Mater.* **2018**, *30* (52), 1801179.
- (4) Wang, L.; Boutilier, M. S. H.; Kidambi, P. R.; Jang, D.; Hadjiconstantinou, N. G.; Karnik, R. Fundamental Transport Mechanisms, Fabrication and Potential Applications of Nanoporous

- Atomically Thin Membranes. Nat. Nanotechnol. 2017, 12 (6), 509-522.
- (5) Bunch, J. S.; Verbridge, S. S.; Alden, J. S.; van der Zande, A. M.; Parpia, J. M.; Craighead, H. G.; McEuen, P. L. Impermeable Atomic Membranes from Graphene Sheets. *Nano Lett.* **2008**, 8 (8), 2458–2462.
- (6) Celebi, K.; Buchheim, J.; Wyss, R. M.; Droudian, A.; Gasser, P.; Shorubalko, I.; Kye, J.-I.; Lee, C.; Park, H. G. Ultimate Permeation across Atomically Thin Porous Graphene. *Science* **2014**, 344 (6181), 289–292.
- (7) Yang, Y.; Yang, X.; Liang, L.; Gao, Y.; Cheng, H.; Li, X.; Zou, M.; Ma, R.; Yuan, Q.; Duan, X. Large-Area Graphene-Nanomesh/Carbon-Nanotube Hybrid Membranes for Ionic and Molecular Nanofiltration. *Science* **2019**, *364* (6445), 1057–1062.
- (8) O'Hern, S. C.; Stewart, C. A.; Boutilier, M. S. H.; Idrobo, J.-C.; Bhaviripudi, S.; Das, S. K.; Kong, J.; Laoui, T.; Atieh, M.; Karnik, R. Selective Molecular Transport through Intrinsic Defects in a Single Layer of CVD Graphene. *ACS Nano* **2012**, *6* (11), 10130–10138.
- (9) O'Hern, S. C.; Boutilier, M. S. H.; Idrobo, J.-C.; Song, Y.; Kong, J.; Laoui, T.; Atieh, M.; Karnik, R. Selective Ionic Transport through Tunable Subnanometer Pores in Single-Layer Graphene Membranes. *Nano Lett.* **2014**, *14* (3), 1234–1241.
- (10) Kidambi, P. R.; Jang, D.; Idrobo, J.-C.; Boutilier, M. S. H.; Wang, L.; Kong, J.; Karnik, R. Nanoporous Atomically Thin Graphene Membranes for Desalting and Dialysis Applications. *Adv. Mater.* **2017**, 29 (33), 1700277.
- (11) Kidambi, P. R.; Nguyen, G. D.; Zhang, S.; Chen, Q.; Kong, J.; Warner, J.; Li, A.-P.; Karnik, R. Facile Fabrication of Large-Area Atomically Thin Membranes by Direct Synthesis of Graphene with Nanoscale Porosity. *Adv. Mater.* **2018**, *30* (49), 1804977.
- (12) Huang, S.; Dakhchoune, M.; Luo, W.; Oveisi, E.; He, G.; Rezaei, M.; Zhao, J.; Alexander, D. T. L.; Züttel, A.; Strano, M. S.; Agrawal, K. V. Single-Layer Graphene Membranes by Crack-Free Transfer for Gas Mixture Separation. *Nat. Commun.* **2018**, 9 (1), 2632.
- (13) He, G.; Huang, S.; Villalobos, L. F.; Zhao, J.; Mensi, M.; Oveisi, E.; Rezaei, M.; Agrawal, K. V. High-Permeance Polymer-Functionalized Single-Layer Graphene Membranes That Surpass the Postcombustion Carbon Capture Target. *Energy Environ. Sci.* **2019**, 12, 3305–3312.
- (14) Boutilier, M. S. H.; Jang, D.; Idrobo, J.-C.; Kidambi, P. R.; Hadjiconstantinou, N. G.; Karnik, R. Molecular Sieving Across Centimeter-Scale Single-Layer Nanoporous Graphene Membranes. *ACS Nano* **2017**, *11* (6), 5726–5736.
- (15) O'Hern, S. C.; Jang, D.; Bose, S.; Idrobo, J.-C.; Song, Y.; Laoui, T.; Kong, J.; Karnik, R. Nanofiltration across Defect-Sealed Nanoporous Monolayer Graphene. *Nano Lett.* **2015**, *15* (5), 3254–3260.
- (16) Jang, D.; Idrobo, J.-C.; Laoui, T.; Karnik, R. Water and Solute Transport Governed by Tunable Pore Size Distributions in Nanoporous Graphene Membranes. *ACS Nano* **2017**, *11* (10), 10042–10052.
- (17) Surwade, S. P.; Smirnov, S. N.; Vlassiouk, I. V.; Unocic, R. R.; Veith, G. M.; Dai, S.; Mahurin, S. M. Water Desalination Using Nanoporous Single-Layer Graphene. *Nat. Nanotechnol.* **2015**, *10* (5), 459–464.
- (18) Mahurin, I.; Shannon, M.; Vlassiouk, I.; Sheng, D.; Surwade, S. P.; Unocic, R. R.; Smirnov, S. Nanoporous graphene membrane for desalination of salt water. **2016**, US14/995,528.
- (19) Gilbert, S. M.; Dunn, G.; Azizi, A.; Pham, T.; Shevitski, B.; Dimitrov, E.; Liu, S.; Aloni, S.; Zettl, A. Fabrication of Subnanometer-Precision Nanopores in Hexagonal Boron Nitride. *Sci. Rep.* **2017**, 7 (1), 15096.
- (20) Wells, D. B.; Belkin, M.; Comer, J.; Aksimentiev, A. Assessing Graphene Nanopores for Sequencing DNA. *Nano Lett.* **2012**, *12* (8), 4117–4123.
- (21) Merchant, C. A.; Healy, K.; Wanunu, M.; Ray, V.; Peterman, N.; Bartel, J.; Fischbein, M. D.; Venta, K.; Luo, Z.; Johnson, A. T. C.;

- Drndić, M. DNA Translocation through Graphene Nanopores. *Nano Lett.* **2010**, *10* (8), 2915–2921.
- (22) Russo, C. J.; Golovchenko, J. A. Atom-by-Atom Nucleation and Growth of Graphene Nanopores. *Proc. Natl. Acad. Sci. U. S. A.* **2012**, 109 (16), 5953–5957.
- (23) Garaj, S.; Hubbard, W.; Reina, A.; Kong, J.; Branton, D.; Golovchenko, J. A. Graphene as a Subnanometre Trans-Electrode Membrane. *Nature* **2010**, *467* (7312), 190–193.
- (24) Rollings, R. C.; Kuan, A. T.; Golovchenko, J. A. Ion Selectivity of Graphene Nanopores. *Nat. Commun.* **2016**, *7*, 11408.
- (25) Kidambi, P. R.; Ducati, C.; Dlubak, B.; Gardiner, D.; Weatherup, R. S.; Martin, M.-B.; Seneor, P.; Coles, H.; Hofmann, S. The Parameter Space of Graphene Chemical Vapor Deposition on Polycrystalline Cu. J. Phys. Chem. C 2012, 116 (42), 22492–22501.
- (26) Kidambi, P. R.; Terry, R. A.; Wang, L.; Boutilier, M. S. H.; Jang, D.; Kong, J.; Karnik, R. Assessment and Control of the Impermeability of Graphene for Atomically Thin Membranes and Barriers. *Nanoscale* **2017**, *9* (24), 8496–8507.
- (27) Kidambi, P. R.; Boutilier, M. S. H.; Wang, L.; Jang, D.; Kim, J.; Karnik, R. Selective Nanoscale Mass Transport across Atomically Thin Single Crystalline Graphene Membranes. *Adv. Mater.* **2017**, 29 (19), 1605896.
- (28) Wang, L.; Drahushuk, L. W.; Cantley, L.; Koenig, S. P.; Liu, X.; Pellegrino, J.; Strano, M. S.; Scott Bunch, J. Molecular Valves for Controlling Gas Phase Transport Made from Discrete Ångström-Sized Pores in Graphene. *Nat. Nanotechnol.* **2015**, *10* (9), 785–790.
- (29) Koenig, S. P.; Wang, L.; Pellegrino, J.; Bunch, J. S. Selective Molecular Sieving through Porous Graphene. *Nat. Nanotechnol.* **2012**, 7 (11), 728–732.
- (30) Molecular structure of Octa Ammonium POSS AM0285 on Hybrid Plastics. https://hybridplastics.com/product/am0285-octaammonium-poss (accessed on Feb 1, 2020).
- (31) Kidambi, P. R.; Mariappan, D. D.; Dee, N. T.; Vyatskikh, A.; Zhang, S.; Karnik, R.; Hart, A. J. A Scalable Route to Nanoporous Large-Area Atomically Thin Graphene Membranes by Roll-to-Roll Chemical Vapor Deposition and Polymer Support Casting. *ACS Appl. Mater. Interfaces* **2018**, *10* (12), 10369–10378.
- (32) Dalwani, M.; Zheng, J.; Hempenius, M.; Raaijmakers, M. J. T.; Doherty, C. M.; Hill, A. J.; Wessling, M.; Benes, N. E. Ultra-Thin Hybrid Polyhedral Silsesquioxane—Polyamide Films with Potentially Unlimited 2D Dimensions. *J. Mater. Chem.* **2012**, 22 (30), 14835—14838
- (33) Zhang, Y.; Benes, N. E.; Lammertink, R. G. H. Visualization and Characterization of Interfacial Polymerization Layer Formation. *Lab Chip* **2015**, *15* (2), 575–580.
- (34) Duan, J.; Litwiller, E.; Pinnau, I. Preparation and Water Desalination Properties of POSS-Polyamide Nanocomposite Reverse Osmosis Membranes. *J. Membr. Sci.* **2015**, *473*, 157–164.
- (35) Ferrari, A. C.; Basko, D. M. Raman Spectroscopy as a Versatile Tool for Studying the Properties of Graphene. *Nat. Nanotechnol.* **2013**, *8* (4), 235–246.
- (36) Kidambi, P. R.; Bayer, B. C.; Blume, R.; Wang, Z.-J.; Baehtz, C.; Weatherup, R. S.; Willinger, M.-G.; Schloegl, R.; Hofmann, S. Observing Graphene Grow: Catalyst—Graphene Interactions during Scalable Graphene Growth on Polycrystalline Copper. *Nano Lett.* **2013**, *13* (10), 4769–4778.
- (37) Cançado, L. G.; Jorio, A.; Ferreira, E. H. M.; Stavale, F.; Achete, C. A.; Capaz, R. B.; Moutinho, M. V. O.; Lombardo, A.; Kulmala, T. S.; Ferrari, A. C. Quantifying Defects in Graphene via Raman Spectroscopy at Different Excitation Energies. *Nano Lett.* **2011**, *11* (8), 3190–3196.
- (38) Lucchese, M. M.; Stavale, F.; Ferreira, E. H. M.; Vilani, C.; Moutinho, M. V. O.; Capaz, R. B.; Achete, C. A.; Jorio, A. Quantifying Ion-Induced Defects and Raman Relaxation Length in Graphene. *Carbon* **2010**, *48* (5), 1592–1597.
- (39) Zhao, J.; He, G.; Huang, S.; Villalobos, L. F.; Dakhchoune, M.; Bassas, H.; Agrawal, K. V. Etching Gas-Sieving Nanopores in Single-Layer Graphene with an Angstrom Precision for High-Performance Gas Mixture Separation. *Sci. Adv.* **2019**, *5* (1), No. eaav1851.

- (40) Cohen-Tanugi, D.; Grossman, J. C. Water Desalination across Nanoporous Graphene. *Nano Lett.* **2012**, *12* (7), 3602–3608.
- (41) Ugeda, M. M.; Fernández-Torre, D.; Brihuega, I.; Pou, P.; Martínez-Galera, A. J.; Pérez, R.; Gómez-Rodríguez, J. M. Point Defects on Graphene on Metals. *Phys. Rev. Lett.* **2011**, *107* (11), 116803.
- (42) Martínez-Galera, A. J.; Brihuega, I.; Gómez-Rodríguez, J. M. Ethylene Irradiation: A New Route to Grow Graphene on Low Reactivity Metals. *Nano Lett.* **2011**, *11* (9), 3576–3580.
- (43) Suk, M. E.; Aluru, N. R. Molecular and Continuum Hydrodynamics in Graphene Nanopores. *RSC Adv.* **2013**, 3 (24), 9365–9372.
- (44) Ren, J.; McCutcheon, J. R. A New Commercial Thin Film Composite Membrane for Forward Osmosis. *Desalination* **2014**, 343, 187–193.
- (45) Cohen-Tanugi, D.; McGovern, R. K.; Dave, S. H.; Lienhard, J. H.; Grossman, J. C. Quantifying the Potential of Ultra-Permeable Membranes for Water Desalination. *Energy Environ. Sci.* **2014**, *7* (3), 1134–1141.
- (46) Deshmukh, A.; Yip, N. Y.; Lin, S.; Elimelech, M. Desalination by Forward Osmosis: Identifying Performance Limiting Parameters through Module-Scale Modeling. *J. Membr. Sci.* **2015**, 491, 159–167.
- (47) Werber, J. R.; Osuji, C. O.; Elimelech, M. Materials for Next-Generation Desalination and Water Purification Membranes. *Nat. Rev. Mater.* **2016**, *1* (5), 16018.
- (48) Molecular sturcture of Trimesoyl chloride on Sigma-Aldrich. https://www.sigmaaldrich.com/catalog/product/aldrich/147532?lang=en&region=US (accessed Feb 1, 2020).
- (49) Chen, L.; Shi, G.; Shen, J.; Peng, B.; Zhang, B.; Wang, Y.; Bian, F.; Wang, J.; Li, D.; Qian, Z.; Xu, G.; Liu, G.; Zeng, J.; Zhang, L.; Yang, Y.; Zhou, G.; Wu, M.; Jin, W.; Li, J.; Fang, H. Ion Sieving in Graphene Oxide Membranes via Cationic Control of Interlayer Spacing. *Nature* **2017**, *550* (7676), 380–383.
- (50) Abraham, J.; Vasu, K. S.; Williams, C. D.; Gopinadhan, K.; Su, Y.; Cherian, C. T.; Dix, J.; Prestat, E.; Haigh, S. J.; Grigorieva, I. V.; Carbone, P.; Geim, A. K.; Nair, R. R. Tunable Sieving of Ions Using Graphene Oxide Membranes. *Nat. Nanotechnol.* **2017**, *12* (6), 546–550.
- (51) Liu, H.; Wang, H.; Zhang, X. Facile Fabrication of Freestanding Ultrathin Reduced Graphene Oxide Membranes for Water Purification. *Adv. Mater.* **2015**, *27* (2), 249–254.
- (52) Ries, L.; Petit, E.; Michel, T.; Diogo, C. C.; Gervais, C.; Salameh, C.; Bechelany, M.; Balme, S.; Miele, P.; Onofrio, N.; Voiry, D. Enhanced Sieving from Exfoliated MoS2Membranes via Covalent Functionalization. *Nat. Mater.* **2019**, *18* (10), 1112–1117.
- (53) Hirunpinyopas, W.; Prestat, E.; Worrall, S. D.; Haigh, S. J.; Dryfe, R. A. W.; Bissett, M. A. Desalination and Nanofiltration through Functionalized Laminar MoS2Membranes. *ACS Nano* **2017**, *11* (11), 11082–11090.